

EFFECTS OF HIGH EXTERNAL PRESSURE ON PHOTONIC CRYSTAL FIBER

M. Shah Alam, N. Somasiri, B. M. A. Rahman, and K. T. V. Grattan

School of Engineering and Mathematical Sciences, City University
Northampton Square, London EC1V 0HB, UK.

E-mail: b.m.a.rahman@city.ac.uk

ABSTRACT

A photonic crystal fiber under high external pressure is analysed by using the finite element method. The effective index, birefringence, mode field profiles, and spot size are calculated and the effect of pressure on these modal properties are discussed for the two fundamental quasi-TE and TM modes. It is seen that the pressure affects all these properties significantly in photonic crystal fibers with both symmetric and asymmetric air holes. Also, it is observed that the two fundamental modes can degenerate at some higher pressure when the air holes are asymmetric.

1. INTRODUCTION

Recently, photonic crystal fibers (PCFs) have attracted much attention because, they exhibit many unique optical properties and a high degree of freedom in design [1]-[2]. PCFs are usually made from a single material, e.g., pure silica, with an array of air holes in the cladding that run along the length of the fiber. The core is a deliberate defect of a missing air hole in the center and light is confined to the core by the index difference between the core and the cladding [1].

The highly-birefringent (hi-bi) fibers or polarization maintaining fibers are very useful as sensing devices and in communication systems [3]. Such fibers eliminate the influence of external parameters (e.g. pressure, temperature, etc) in unstable environments and are capable to preserve the polarization states. It is very important to realize the polarization properties of PCF under those circumstances in order to fully understand the feasibility of using PCFs as sensors for hydrostatic or acoustic pressure, and in underwater communication systems. So, the effect of uniform pressure on the modal interference would be addressed in this work.

In this paper, the finite element method (FEM) [4] is used to perform the stress analysis of a simple hexagonal photonic crystal fiber and then a vector finite element method (VFEM) [5] is used to find the modal solutions and the effects of high external pressure on effective index, modal profiles, birefringence and spot-size of PCF are shown.

2. THEORY

Most of the research into this new class of fibers are based on experiments [1], which are recently complemented by various numerical analyses. Among the numerical techniques, the effective index method [6], the plane wave expansion method [7], a boundary element method [8], a finite difference approach [9], etc, have been used. However, most of the numerical analyses are dedicated only to the modal solutions of unstressed fibers. As a matter of fact, for accurate determination of modal characteristics of stressed fibers, one needs to solve the full vectorial wave equations.

Among the full vectorial approaches used in modelling PCFs, the finite element based approaches [10], [11] have been developed to study modal properties of unstressed PCFs. These approaches are very useful and efficient. However, as to the author's best knowledge, the effect of external pressure on the modal properties of a PCF has not yet been addressed using this versatile and rigorous numerical analysis technique. Only, recently, Zhu and Brown [12] reported the stress-induced birefringence in microstructured fiber under lateral force and twist. So, in this work, the effects of uniform external pressure on modal properties of an hexagonal photonic crystal fiber are shown for the first time.

The birefringence in a hi-bi fiber is usually introduced by the thermal and the mechanical properties of different regions and by their geometric

parameters. In a PCF, unlike the standard hi-bi fibers, the birefringence is mainly attributed by geometric anisotropy. But, in this case, i.e., under external pressure, the fiber will be deformed and a stress distribution will be formed in the fiber. Then as a result of the elasto-optic effect, stress induces anisotropic changes of the refractive index within the fiber and thus creates birefringence.

To include the external pressure effect in the stress analysis using the FEM, a triangular element topology is used and a linear equation system is solved, and using the techniques described in [4], [13], one can easily obtain strain vector, stress vector in each element and finally the refractive index due to the elasto-optic effect in each element using the following equations [4]:

$$n_x = n_{x0} - C_1\sigma_x - C_2(\sigma_y + \sigma_z) \quad (1)$$

$$n_y = n_{y0} - C_1\sigma_y - C_2(\sigma_x + \sigma_z) \quad (2)$$

$$n_z = n_{z0} - C_1\sigma_z - C_2(\sigma_x + \sigma_y) \quad (3)$$

Here C_1 , C_2 are the elasto-optic coefficients of the fiber material and σ_x , σ_y , and σ_z are the stress components in x , y , and z directions, respectively. n_{x0} , n_{y0} , and n_{z0} are the unstressed refractive indices of the material. n_x , n_y , and n_z are the main diagonal elements of the anisotropic refractive index tensor. Once the stress analysis is performed, the anisotropic refractive index components are calculated using (1)-(3), and the vector finite element method [11] is then employed to find the modal solutions of quasi-TE (H_{11}^y) and quasi-TM (H_{11}^x) modes. The details of the vector FEM can be found in the literature, [5].

3. RESULTS

First, an unstressed PCF is considered, when external pressure is zero and the two fundamental propagation modes are found for different pitches, Λ , which is the center-to-center distance between two adjacent holes. Because of the symmetry nature of the structure, only one-quarter of the fiber cross section is divided into triangular elements and thus the computational cost is reduced and adequate mesh refinement in the core region is achieved. Fig. 1 shows the effective index versus pitch for different air hole diameters. Here, the refractive index of fiber material, $n = 1.45$, effective index, $n_e = \beta/k_0$, where β is the phase constant and k_0 is the free space wavenumber. Solid and dashed lines show the variations of effective indices of the fundamental quasi-TM (H_{11}^x) and quasi-TE (H_{11}^y) modes,

respectively, when the operating wavelength $\lambda = 1.55\mu\text{m}$. Here, both symmetric (i.e., all air holes having same diameter, d) and asymmetric (i.e., air holes having unequal diameters, d_1 and d_2 as shown in the inset) air holes are considered. For symmetric air holes, two cases with d equals $3\mu\text{m}$ and $5\mu\text{m}$ are considered. In these cases, the two polarization modes are nearly degenerate and in the figure the curves are just overlapping. The result is compared with that of Koshiba and Saitoh [10] for a hole diameter, $d = 5\mu\text{m}$ and a pitch, $\Lambda=6.75\mu\text{m}$, and a very good agreement is observed. It can be seen that at some fixed value of pitch, with the increase in hole diameter the effective index reduces. This is due to the fact that with the increase in hole diameter the equivalent index of the air-hole cladding region is reduced, which increases index contrast between the effective core and cladding.

For asymmetric hole diameters, it can be observed that when $d_1 = 3\mu\text{m}$ and $d_2 = 5\mu\text{m}$, the index values lie between $d = 3\mu\text{m}$ and $d = 5\mu\text{m}$, but when $d_1 = 3\mu\text{m}$ and $d_2 = 6\mu\text{m}$, the index values are smaller than those of $d = 5\mu\text{m}$. Also, when there are asymmetric holes in the structure, the polarization modes are non-degenerate and gives rise to larger values of birefringence at smaller values of pitch. In all these cases effective index increases with the increase in separation between the holes. This arises because, with the fixed hole size, an increase in the spacing between the holes increases the fill factor, and so the equivalent index of the cladding increases. However, as the equivalent index of cladding increases, but the core index value remains constant, the index contrast between core and cladding is reduced with the increase in separation between the holes. The variations of the spot-size with the separation between holes for the fundamental modes are shown in Fig. 2. Here, the spot-size area is defined as the guide area where the field intensity is at least $1/e^{\text{th}}$ the maximum intensity. It can be observed that with the increase in the separation, the spot-size area increases for all the hole diameters. For a fixed pitch, larger air hole pushes the modal field to be more confined reducing the spot-size area and smaller air-holes allow modal field to leak through silica bridge enlarging the spot-size area. All these can also be realized from the modal field profiles shown in Fig. 3.

The dominant H_x modal field profiles of H_{11}^x mode is shown in Fig. 3, in the case of symmetric air holes, $d_1 = d_2 = 5\mu\text{m}$, when the fiber is unstressed, i.e., the external pressure is zero. Figs. 3(a) and 3(b)

show the field profile at a pitch, $\Lambda = 6.75\mu\text{m}$ and $\Lambda = 8.0\mu\text{m}$, respectively. At smaller value of pitch, the field is more confined. From these figures, it can be clearly seen that the field expands and leak through the silica bridge when the pitch is larger.

Now, pressure is applied to the PCF with symmetric air holes. Fig. 4 shows effective index versus pressure when operating wavelength, $\lambda = 1.55\mu\text{m}$ and pitch, $\Lambda = 6.75\mu\text{m}$. It can be observed that with the application of pressure, the effective index significantly changes for both the fundamental modes. The x -polarized fundamental mode (H_{11}^x mode) gets higher effective refractive index at high pressure. At zero pressure, the modes are degenerate, but as the pressure increases, the degeneracy gets lost, and the birefringence increases more when the hole diameter is larger. At 1500 MPa, when $d = 5\mu\text{m}$, the birefringence is about 16 times larger than that of $d = 3\mu\text{m}$. The pressure induced waveguide deformation increases with the air hole fraction, thereby making stress birefringence more severe when air holes are larger.

Finally, the effect of pressure on a PCF with asymmetric air holes is observed. Two cases are considered with $d_1 = 3\mu\text{m}$, $d_2 = 4\mu\text{m}$ and with $d_1 = 3\mu\text{m}$, $d_2 = 6\mu\text{m}$. Operating wavelength, $\lambda = 1.55\mu\text{m}$ and pitch, $\Lambda = 6.75\mu\text{m}$. For asymmetric air holes, significant birefringence exists even when pressure is zero and this can be clearly seen in Fig. 5, where the birefringence versus pressure is plotted. For the first case, it can be seen that the two linearly polarized waves degenerate, i.e. $B=0$, at around 850 MPa. However, for the other case, the birefringence value is much higher and it decreases slowly between the range of pressure considered here, and may degenerate at some higher value of pressure. The value of the critical pressure, when the modes degenerate, as shown in Fig. 5, plays an important role in polarization maintaining applications.

4. CONCLUSION

The finite element method is efficiently applied to find the modal properties of PCFs under high external pressure. Initially, the stress analysis is carried out and the anisotropic refractive index due to elasto-optic effect is calculated. Then a vector finite element method is employed to find the effective index, birefringence, mode field profiles, and spot size for the two fundamental quasi-TE and TM modes and the effect of pressure on these modal properties are discussed. It is seen that the pressure

affects all these properties significantly in photonic crystal fibers with both symmetric and asymmetric air holes. For PCFs with symmetric air holes, the modes are nearly degenerate, but with the increase in pressure, the modes are seen to become non-degenerate. However, for PCFs with asymmetric air holes, the modes are non-degenerate when the pressure is zero, but it is observed that the two modes can degenerate at some higher value of pressure.

REFERENCES

- [1] J. C. Knight, T. A. Birks, P. St. J. Russell, and D. M. Atkin, "All-silica single-mode optical fiber with photonic crystal cladding," *Opt. Lett.*, vol. 21, pp. 1547—1549, Oct. 1996.
- [2] J. C. Knight, "Photonic crystal fibers," *Nature*, vol. 424, no. 14, pp. 847—851, Aug. 2003.
- [3] J. R. Clowes, S. Syngellakis, and M. N. Zervas, "Pressure sensitivity of side-hole optical fiber sensors," *IEEE Photon. Technol. Lett.*, vol. 10, pp. 857—859, June 1998.
- [4] K. Okamoto, T. Hosaka, and T. Eda, "Stress analysis of optical fibers by a finite element method," *IEEE J. Quantum Electron.*, vol. QE-17, pp. 2123—2129, Oct. 1981.
- [5] B. M. A. Rahman and J. B. Davies, "Finite-element solution of integrated optical waveguides," *J. Lightwave Technol.*, vol. 2, pp. 682—688, Oct. 1984.
- [6] T. A. Birks, J. C. Knight, and P. St. J. Russell, "Endlessly single-mode photonic crystal fiber," *Opt. Lett.*, vol. 22, pp. 961—963, July 1997.
- [7] A. Ferrando, E. Silvester, J. J. Miret, P. Andrés, and M. V. Andrés, "Full vector analysis of a realistic photonic crystal fiber," *Opt. Lett.*, vol. 24, no. 5, pp. 276—278, 1999.
- [8] N. Guan, S. Habu, K. Takenaga, K. Himeno, and A. Wada, "Boundary element method for analysis of holey optical fibers," *J. Lightwave Technol.*, vol. 21, pp. 1787—1792, Aug. 2003.
- [9] Z. Zhu and T. G. Brown, "Full-vectorial finite-difference analysis of microstructured optical fibers," *Optics Express*, vol. 10, no. 17, pp. 853—864, Aug. 2002.
- [10] M. Koshiba and K. Saitoh, "Numerical verification of degeneracy in hexagonal photonic crystal fibers," *IEEE Photon. Technol. Lett.*, vol. 13, pp. 1313—1315, Dec. 2001.
- [11] B. M. A. Rahman, A. K. M. S. Kabir, M. I. Ahmed, M. Rajarajan, and K. T. V. Grattan, "Modal solutions of photonic crystal fibers by the finite element method," *Proceedings of Photonics EUROPE*, April 2004, paper no. 5450-27, Strasbourg, France.
- [12] Z. Zhu and T. G. Brown, "Stress-induced birefringence in microstructured optical fibers," *Opt. Lett.*, vol. 28, pp. 2306—2308, Dec. 2003.
- [13] Y. Liu, B. M. A. Rahman, and K. T. V. Grattan, "Thermal-stress-induced birefringence in bow-tie optical fibers," *Applied Opt.*, vol. 33, pp. 5611—5616, Aug. 1994.

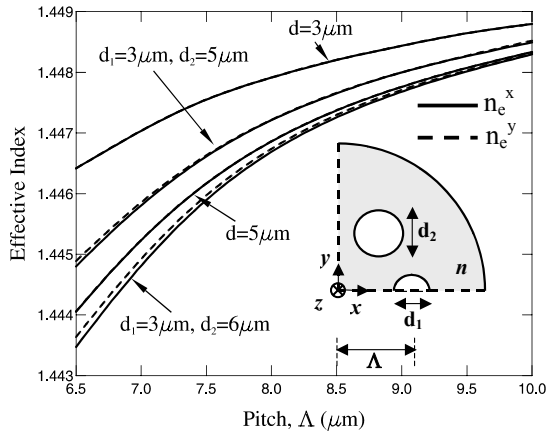


Fig. 1 Variation of effective index with pitch.

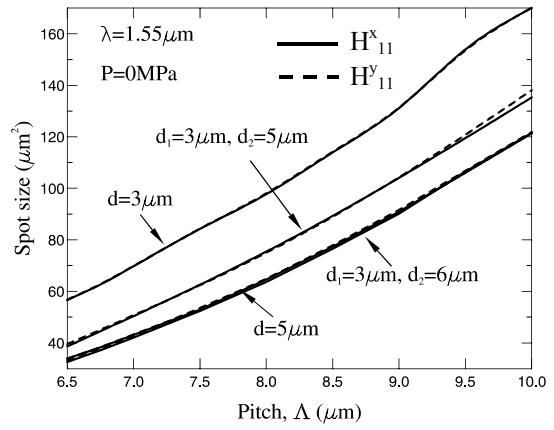
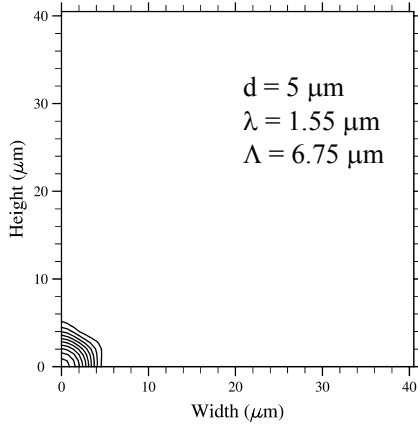
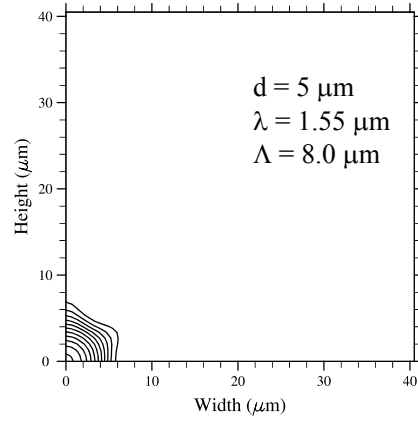


Fig. 2 Variation of spot size with pitch.



(a)



(b)

Fig. 3 Mode field profiles of the quasi-TM mode of unstressed PCF with symmetric air holes.

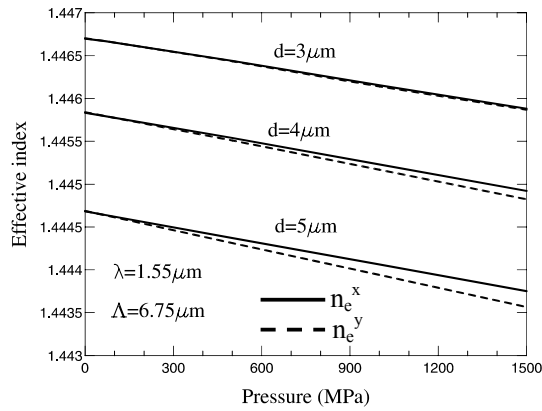


Fig. 4 Variation of effective index with pressure.

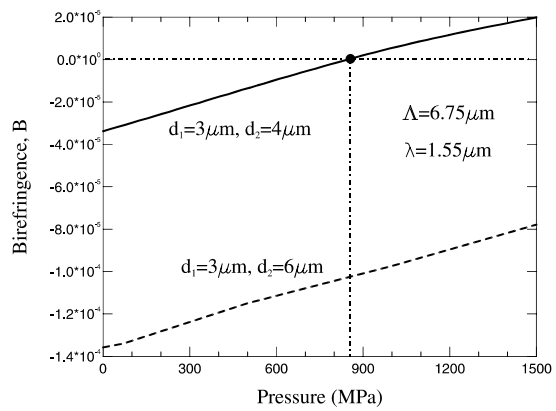


Fig. 5 Variation of birefringence with pressure.